The Electrochemical Behavior of Polyimide Binders in Li and Na Cells

The Electrochemical Behavior of Polyimide Binders in Li and Na Cells

B. N. Wilkes,[a] Z. L. Brown,[a,*] L. J. Krause,[b,] M. Triemert,[c] and M. N. Obrovac[a,**,z]**

[a]*Department of Chemistry, Dalhousie University, Halifax, Nova Scotia B3H 4R2, Canada*
[b]*Corporate Research Materials Laboratory, St. Paul, Minnesota 55144, USA*
[c]*Electronics Markets Materials Division, St. Paul, Minnesota 55144, USA*

The electrochemistry of aromatic and aliphatic polyimide binders was characterized in composite coatings for Li-ion and Na-ion battery negative electrodes. Aromatic polyimide was found to have a large first lithiation capacity of 1943 mAh/g and a reversible capacity of 874 mAh/g in lithium cells. The large first lithiation capacity is suggestive of its full reduction to carbon. Subsequent cycles of aromatic-PI are also similar to that of hydrogen containing carbons. Aromatic-PI is also active in Na cells, but with less capacity and less hysteresis during cycling, which is also consistent with the behavior of hydrogen containing carbon in Na cells. Therefore, we suspect that after the first lithiation or sodiation, all of the aromatic-PI becomes carbonized. These conductive reaction products lead to excellent cycling in alloy cells. In contrast, aliphatic-PI is inert and leads to poor cycling when used in alloy cells. These results may have large implications for the use of conductive polymer binders, which may just be carbonizing during their first lithiation.

Manuscript submitted September 16, 2015; revised manuscript received November 2, 2015. Published December 9, 2015.

It has been shown that effective binders for alloy negative electrodes should possess specific qualities. These are: good adhesion to both the alloy particles and current collector, complete surface coverage of the alloy particles to reduce electrolyte decomposition, and the ability to tolerate volume expansion by stretching or self-healing to maintain the structural integrity of composite coatings.[1] In addition to these qualities, studies have shown that alloy negative electrodes using conductive polymer binders can achieve enhanced cycling performance due to the binder providing a conductive network that maintains electrical connectivity between the constituent electrode particles. For example, Wu et al. showed that incorporating a conducting polymer hydrogel into a Si-based anode resulted in a cycle life of 5000 cycles with over 90% capacity retention.[2]

Aromatic polyimides (aro-PI) have been found to be excellent binders for alloy negative electrodes.[3–5] Polyimide (PI) binders are prepared from poly(amic acids), which are then cured to imidize the poly(amic acid) to PI by a condensation reaction, as shown in Figure 1. The imidization step can occur between 250–400°C and typically lasts one hour.[6–8] Polyimide binder demonstrates flexibility, good surface coverage and strong adhesion to current collectors.[5,7] The strong adhesion force between PI and current collectors or alloy particles arises from the carboxylic groups of the poly(amic acid) (PI precursor) interacting with metal surfaces. For example, poly(amic acid) reacts with copper to make copper carboxylate, which inhibits imidization so the interaction remains after curing.[9] This results in good adhesion between PI binders and the current collector. Similarly, the silanol groups (Si-OH) on the surface of silicon can react with the carboxylic acid groups of poly(amic acid) to form strong ester-like bonds with Si alloys, as shown in Figure 2.[10,11]

It is well known from classical electrochemistry measurements, that aro-PI can undergo reversible reduction/oxidation reactions at the diimide functional group (part of the π-system).[8] When immersed in aprotic solvents, PI films demonstrate a 2–3 electron reduction, depending on the type of PI.[8,12] This corresponds to a specific capacity of about 110–165 mAh/g. This electrochemical behavior must be accompanied by electrolyte (ion) transport through the film to maintain charge balance. The reduced forms of PI are air stable and can be electronically conducting.[8] However, these classical electrochemical experiments were performed on thick films (i.e. thick compared to the ~20 nm thickness of PI on a particle in a composite coating) of about 0.1–12 μm and at voltages no more reducing than about 1.3 V vs. Li/Li^+.

As a consequence of their electrochemical activity, aro-PI binders have been found to contribute additional reversible capacity to negative electrodes in Li-ion cells and can contribute significantly to reversible and irreversible anode capacity. Ohta et al. found that 3,3',4,4'-biphenyltetracarboxylic dianhydride 4,4'-oxydianiline (BPDA-ODA) PI contributed 63.3 and 28.6 mAh/g of additional discharge and charge capacity in graphite coatings, respectively, in the first cycle compared to PVDF.[13] This electrochemical activity of aro-PI was claimed to be due the known 2-electron reduction of PI and the PI capacity was shown to increase with increasing carbonyl oxygen. However, it is easy to compute that the PI would have to have a first discharge and first charge capacity of about 1200 mAh/g and 540 mAh/g, respectively, to result in the increased capacity they observe. This capacity is an order of magnitude larger than the capacity from a 2-electron reduction. Similarly, Liu et al. reported that aro-PI has a high irreversible capacity of about 1000 mAh/g. In contrast, Choi et al. used Fourier transform infrared analysis of Si electrodes with aro-PI binders at different states of charge. At 5 mV they found that the aro-PI had undergone a single electron reduction at the carbonyl oxygen atoms of the diimide ring,[14] corresponding to a capacity of only 110 mAh/g.

In this study, the electrochemistry of aro-PI and ali-PI binders in Li and Na cells is explored. To our knowledge, the electrochemistry of aliphatic PI (ali-PI) has not been reported. Both aro-PI and ali-PI adhere to and uniformly cover metal surfaces by the same mechanism. Therefore studying the difference between the electrochemistry of aro-PI and ali-PI will allow the importance of aromaticity toward the cycling performance of PI to be better understood. In addition, the electrochemistry of PI in Na-cells and the importance of the cation on PI performance, which has also not been previously explored, will be discussed.

Experimental

Poly(amic acids).— Poly(amic acids) were prepared using procedure modified from that described by Krause et al.[15] To prepare the aro-poly(amic acid), 4,4′-oxydianiline (97% Aldrich) and 3,3′,4,4′-benzophenonetetracarboxylic dianhydride (97+% Alfa Aesar) were dissolved in NMP in a 1:1 molar ratio and mixed overnight by tumbling in a 250 mL Nalgene bottle with ~200 g of $\frac{1}{4}''$ stainless steel balls.

*Electrochemical Society Student Member.
**Electrochemical Society Active Member.
[z]E-mail: mnobrovac@dal.ca

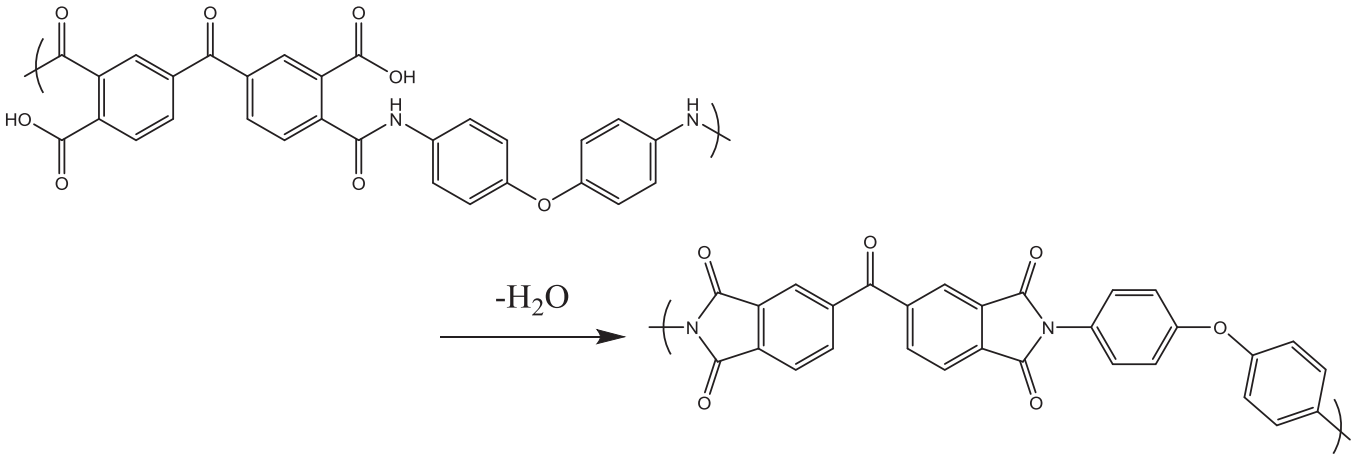

Figure 1. Imidization of poly(amic acid) to polyimide.

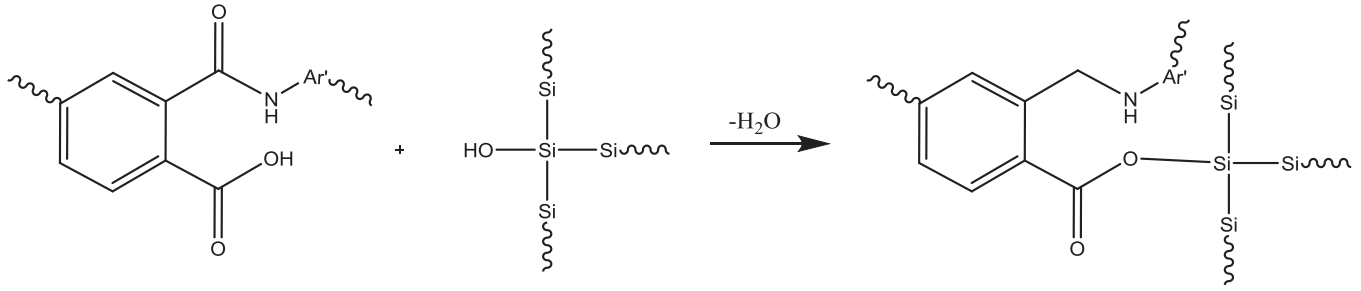

Figure 2. Mechanism by which poly(amic acid) adheres to silicon surfaces.

After tumbling a clear, yellow solution of poly(amic acid) was obtained. In the same way, ali-poly(amic acid) was prepared by dissolving 4,4'-diaminodicyclohexylmethane (98+% Alfa Aesar, mixture of stereoisomers) in NMP before adding 1,2,3,4-butanetetracarboxylic dianhydride (≥94% Aldrich) with further mixing. A clear or sometimes cloudy white solution was obtained. However, it was found that the cloudiness of the solution did not affect the electrochemistry of the resulting ali-PI.

Electrode preparation.— Electrode coatings were made by mixing active material, binder and, if required, carbon black (Super P, Erachem Europe) in N-methyl-2-pyrrolidone (NMP, Sigma Aldrich, anhydrous 99.5%) in specific ratios according to Table I. Coating slurries were mixed for one hour in a Retsch PM200 planetary mill at 100 rpm with four $\frac{1}{2}''$ tungsten carbide balls and then spread onto copper foil with a $0.004''$ doctor blade. Coatings were dried in air at 120°C for one hour, except those containing hard carbon, which were dried under vacuum at 80°C for 30 minutes. Coatings containing poly(amic acids) were imidized at 300°C under an argon atmosphere for one hour. The active materials used were 3M L-20772 V6 Si alloy (hereafter denoted V6, 3 μm, from 3M Co., St. Paul, MN), graphite (MAG-E Hitachi or SFG6L Timcal), hard carbon (preparation details below) and Sb/C nanocomposite (preparation details below). TiN (99.7% Alfa Aesar) was used as an inert conductive filler in some electrodes in order to measure the electrochemistry of the binder without the presence of an active material. The binders used were polyvinylidene fluoride resin (HSV 900 Kynar, hereafter denoted PVDF), ali-PI and aro-PI (imidized from their poly(amic acids), as described above).

Coin cell preparation.— Circular electrodes with an area of 1.3 cm^2 were punched from the electrode coatings. Typical active material loadings were about 0.85 mAh/cm^2; except for Sb/C and TiN electrodes, where the loadings were 0.15 mA/cm^2 and 0.4 mAh/cm^2, respectively. Because TiN is inert, the active material loading for TiN electrodes was calculated based on the mass of the binder, assuming a binder capacity of 1000 mAh/g. Coin cells were assembled in an argon-filled glove box. Either lithium (99.9%, Sigma Aldrich) or sodium metal foil (cold-rolled from Na ingot, Sigma Aldrich, ACS reagent grade) were used as counter electrodes. Two layers of Celgard 2301 and one layer of polypropylene blown microfiber (3M Company) were used as separators. 1M $LiPF_6$ or 1M $NaPF_6$ (Sigma Aldrich 98%) in a solution of ethylene carbonate, diethyl carbonate and monofluoroethylene carbonate (EC/DEC/FEC; 3:6:1 by mass, all from BASF) were used as electrolytes except with hard carbon where EC/DEC (1:2 by volume, also from BASF) was used. Coin cells were cycled on either a Maccor Series 4000 Automated Cycler or Neware

Table I. Electrode formulations used in this study.

Coating Components	Volume Ratio	Weight Ratio	Binders Used
MAG-E/carbon black/oxalic acid/binder	90/0.5/0.6/9	93/0.5/0.5/6	PVDF, aro-PI, ali-PI
V6/carbon black/binder	58.4/22.6/19.0	73.2/17.5/9.3	aro-PI, ali-PI
V6/SFG6L/carbon black/binder	44.6/33.8/2.4/19.1	60/28/2/10	aro-PI
TiN/binder	83/17	95/5	PVDF, aro-PI, ali-PI
hard carbon/carbon black/binder	80/12/8	82.4/12.4/5.2	PVDF, aro-PI
(Sb/C)/carbon black/binder	80/10/10	90.1/6.1/3.8	aro-PI

Table II. Cycling protocols for cells in this study.

Active Material	Voltage Range (V)	Discharge Rate	Charge Rate	C (mAh/g)
Graphite	0.005–2	C/5, Trickle C/10	C/5	370
V6 (and V6/graphite)	1st cycle: 0.005–1.5, Other: 0.005–0.9	1st cycle: C/10, Trickle C/40, Other: C/4, Trickle C/20	1st cycle: C/10, Other: C/4	950 (760)
binder in TiN/binder	0.005–2	C/25, Trickle C/50	C/25	1000
hard carbon	0.005–2	C/10, Trickle C/20	C/10	300
Sb in Sb/C	0.005–2	C	C	660

Battery Testing System. The cycling protocols used to test cells are listed in Table II.

Hard carbon preparation.— Glucose (96% Aldrich) was dewatered by heating overnight at 180°C in air. The dewatered glucose was then heated to 100°C under Ar flow for one hour, followed by a 1°C/min ramp to 700°C, and was then held at this temperature for 10 hours. The resulting carbon was cooled to room temperature, ground by hand and passed through a 75 μm sieve before another heat-treatment to 1100°C for one hour under flowing argon. The hard carbon was transferred without air exposure into an argon-filled glove box.

Sb/C nanocomposite preparation and characterization.— The Sb/C nanocomposite was prepared as outlined by Qian et al.[16] Antimony powder (99.5% Sigma Aldrich, −100 mesh) was ball milled for 11 hours under argon atmosphere with carbon black (Super P, Erachem Europe) in a mass ratio of 7:3; the weight ratio of the milling balls (stainless steel, $\frac{1}{2}''$) to the powders was 20:1. The crystalline structure of the nanocomposite was characterized by X-ray powder diffraction (XRD) using a Rigaku Ultima IV X-Ray Diffractometer, equipped with a D/Tex Ultra linear detector with K-beta filter. For XRD measurements, the sample was loaded into a gastight X-ray sample holder (Mylar cover) in an argon-filled glove box.

Field emission electron microscopy measurements.— Bulk TiN/PI electrode coatings of various compositions were polished using a JEOL IB-19500CP cross-section polisher. The polished electrodes were then imaged with a JEOL JSM-7600F field emission electron microscope (FEM) using a low-angle backscattered electron (LABE) detector. The area fraction of TiN particles in the electrode coating was estimated using ImageJ software,[17] with a minimum of four cross-section images examined for each electrode composition.

Results

aro-PI, ali-PI, and PVDF binder electrochemistry in composite coatings.— TiN/binder coatings were prepared in order to investigate the electrochemistry of binders in the same morphology as they are used in composite coatings. TiN is electrochemically inactive and electronically conductive.[18,19] Therefore, such electrodes should be

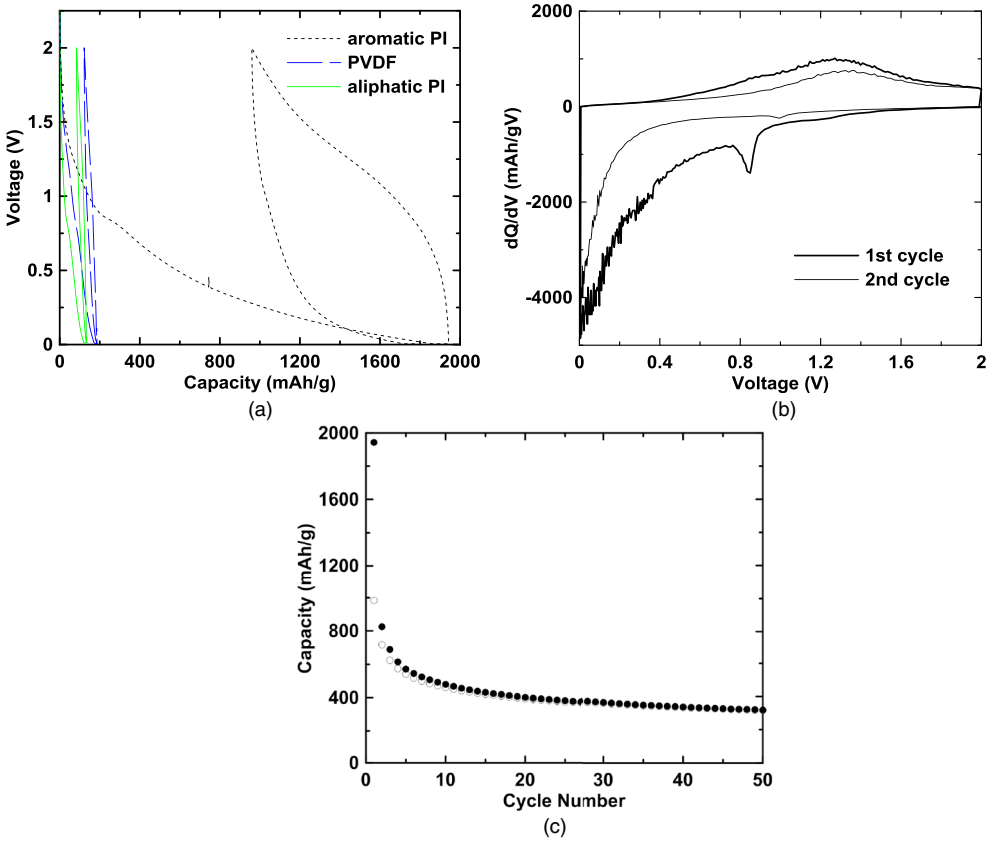

Figure 3. (a) Voltage curves of aro-PI, ali-PI and PVDF binders versus Li-metal as measured in a TiN/binder composite coating. (b) Differential capacity curve of aro-PI versus Li-metal as measured in a TiN/aro-PI composite coating. The first cycle is shown in bold. (c) Cycling performance of aro-PI versus Li-metal as measured in a TiN/aro-PI composite coating.

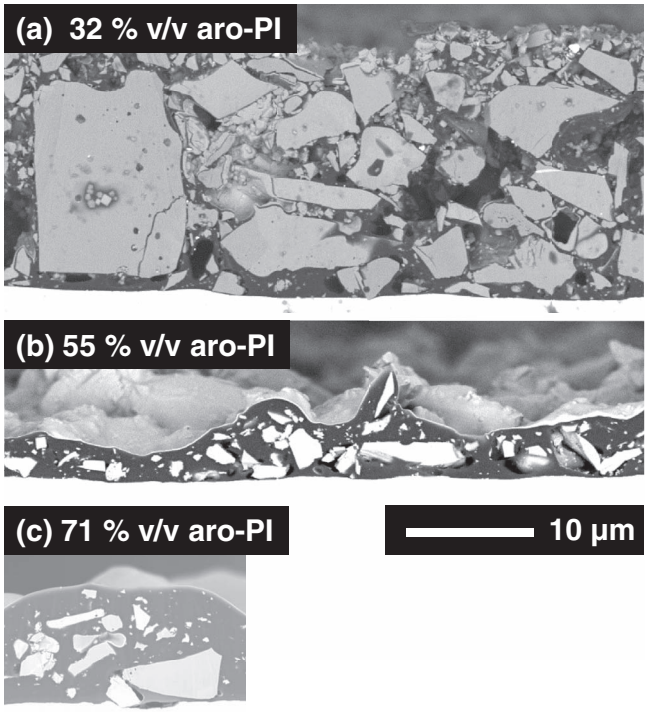

Figure 4. Cross section FEM image of TiN/aro-PI electrodes with (a) 32%, (b) 55%, and (c) 71% by volume aro-PI binder.

good research vehicles to enable the measurement of binder electrochemistry, as they are present in composite coatings. We believe such coatings represent a better analogue for binders in composite coatings than electrodes made by spin-coating a thin layer of binder on a smooth substrate. In addition, because of the available surface area of TiN powder, the use of TiN/binder composite coatings allows a much larger binder mass to be investigated than is possible with spin-coated thin film electrodes. Figure 3a shows the first-cycle voltage curves of aro-PI, ali-PI and PVDF binders in TiN/binder coatings versus Li-metal where the TiN/binder ratio is 83/17 v/v. The initial lithiation capacity of aro-PI is 1873 mAh/g and the aro-PI first-cycle reversible capacity is 1000 mAh/g. Both of these values are much larger than those of PVDF or ali-PI, which are essentially inactive. Figure 3b shows the differential capacity curve of aro-PI. The small irreversible peak near 0.9 V that occurs initially is likely due to electrolyte decomposition reactions during the formation of the solid electrolyte interphase (SEI). A plateau at this voltage is present in Figure 3a for all of the binders; however, the 0.9 V plateau capacity is much larger for aro-PI. The lithiation of aro-PI then occurs during a broad peak that is truncated at 0 V, while the delithiation capacity occurs over a broad anodic peak centered at about 1.25 V. Subsequent cycles resulted in a rapid decay of capacity. The cycling performance of aro-PI is shown in Figure 3c. After initial rapid capacity fade, the capacity stabilizes and becomes about 350 mAh/g by 50 cycles.

In order to see the effect of electrode formulation on aro-PI electrochemistry a number of different TiN/aro-PI electrodes with different coating formulations were made. Cross-section FEM images of the TiN/aro-PI 68/32, 45/55, and 29/71 v/v coatings are shown in Figure 4. The aro-PI coats most of the TiN particles and is dense. However, there are some occlusions in the form of $\approx$ 1 µm voids. Figure 5a shows the cycling performance of aro-PI in TiN/aro-PI coating formulations with aro-PI contents from 17–71 volume %. There is significant variation in irreversible capacity, reversible capacity and fade rate with the aro-PI binder content. Coatings with the smallest amount of aro-PI binder had the highest capacities while coatings with a larger amount of aro-PI binder had the highest initial fade rate.

Figure 5b shows a plot of the average first lithiation capacity versus the volume percent of aro-PI in the TiN/aro-PI coating. As the aro-PI content of the coating increases, the first lithiation capacity is reduced. Above an aro-PI content of 63 vol. %, the aro-PI becomes inactive. Considering that aro-PI becomes electrically conducting when reduced,[8] the volume fraction at which aro-PI becomes inactive is likely that at which TiN no longer forms electrically conducting paths to the electrode surface in contact with the electrolyte. This would occur when the TiN no longer forms a percolating network throughout the coating. Indeed, no percolating electrically conducting paths from the current collector to the electrode surface are apparent in the FEM image of the 71% v/v aro-PI coating, shown in Figure 4c. Therefore it is understandable why this electrode should be inactive. This concept is illustrated in Figure 6. Figure 6a shows how aro-PI at the electrode surface near an electronically percolating TiN network might begin to reduce. After the reduction at this interface, Figure 6b shows how the aro-PI reduction reaction front can spread, since the reduction products of PI are conductive to both electrons and Li^+ ions. The average aro-PI thickness on the TiN particles at which the electrodes become inactive can be roughly estimated from the PI volume fraction and the measured TiN BET surface area of 1.24 m^2/g. This results in an average geometrical aro-PI thickness of 350 nm for the TiN/aro-PI 37/63 v/v coating, above which the aro-PI becomes inactive. However, this is only a rough estimate of the aro-PI average thickness because of the presence of voids.

The large first lithiation and reversible capacity of aro-PI observed for the active aro-PI coatings cannot be explained by the simple

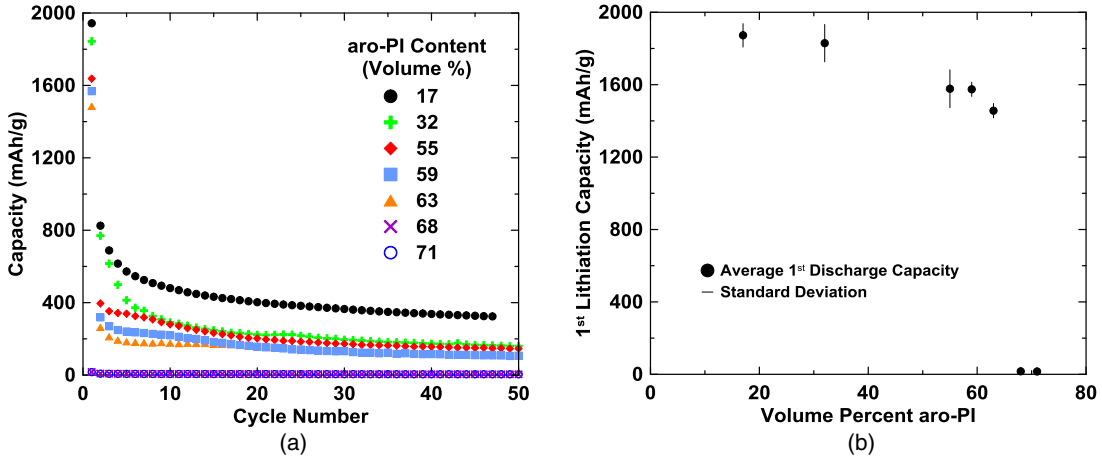

Figure 5. (a) Cycling performance of aro-PI in TiN/aro-PI composite coatings vs. Li with different aro-PI contents, as indicated. (b) Average 1st lithiation capacity versus aro-PI content on TiN particles for the a TiN/aro-PI composite coatings shown in Figure 7a.

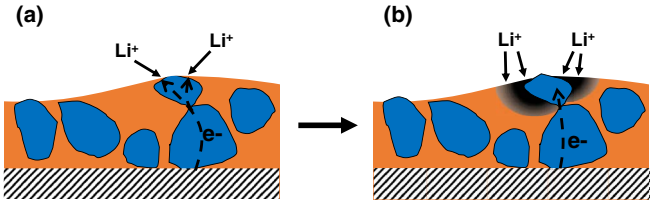

Figure 6. Illustration of how electrochemical aro-PI reduction can occur in a composite coating that provides percolating paths for electrons to reach the coating surface. (a) aro-PI in contact with the electrolyte and with particles that have access to electrons from the current collector can become reduced. (b) Once some aro-PI has become reduced, the reduction reaction front can spread, since the reduction products of aro-PI are conductive to both electrons and Li^+ ions.

2–3 electron reduction observed in previous studies,[8,12] which would correspond to a capacity of only 110–165 mAh/g. Instead, the first lithiation and reversible capacities observed for aro-PI vs Li-metal in Figure 3 of 1943 mAh/g and 874 mAh/g, respectively, correspond to a 35 and a 16 electron reduction, respectively. It is difficult to conceive of a mechanism to account for the uptake of so many lithium atoms, unless the PI is being decomposed. For instance, the complete reduction of aro-PI by Li is:

$$C_{29}O_6H_{14}N_2 + 36.8Li^+ + 36.8e^- \rightarrow 4.8LiC_6 + 14LiH + 6Li_2O + 2Li_3N \quad [1]$$

This represents a 36.8 electron reduction, which is close to the observed 35 electron reduction observed for aro-PI. This is rather convincing evidence that a reaction similar to the total decomposition of aro-PI must occur during the first lithiation. However, although reaction 1 explains the aro-PI first lithiation capacity well, it does not explain its large reversible capacity corresponding to the removal of 16 Li. Instead, we speculate that a more likely mechanism is the formation of a hydrogen containing carbon during aro-PI lithiation according to:

$$C_{29}O_6H_{14}N_2 + 34Li^+ + 34e^- \rightarrow 4.8Li_{3.3}C_6H_{2.3} + 1.4H_2 + 6Li_2O + 2Li_3N \quad [2]$$

Here the total capacity from the hydrogen containing carbon was chosen to be 16Li, in order to correspond to the observed first delithiation capacity of aro-PI. The hydrogen containing carbon lithiation level is according to the model of Zheng and Dahn, where carbon can reversibly form LiC_6 and each hydrogen results in the uptake of an additional lithium.[20] Reaction 2 has more realistic products than Reaction 1 and corresponds to a 34 electron reduction and a 16 electron reversible capacity, which is almost exactly what is observed. Moreover, the voltage curve in Figure 3 is similar to that observed by Zheng and Dahn for hydrogen-containing carbons.[20] Such carbons show large hysteresis, indicating the presence of residual hydrogens terminating the aromatic fragments in the carbon matrix. This hysteresis is believed to occur as a result of lithium ions binding to the edge carbons, which cause them to change their bond hybridization from sp^2 to sp^3.[20] Hydrogen containing carbons also exhibit large capacity fade.[20] Earlier electrochemical measurements of aro-PI did not expose the PI to voltages lower than 1.2 V vs lithium.[8,12] Therefore, the full reduction of aro-PI was not observed in these studies.

As with lithium, it is useful to isolate the capacity arising from the aro-PI when it is used as a binder in sodium cell negative electrodes. Figure 7a shows the voltage profile of aro-PI, ali-PI and PVDF binders in TiN/binder 83/17 v/v composite coatings vs. Na-metal. The differential capacity of aro-PI is shown in Figure 7b. Similar to the

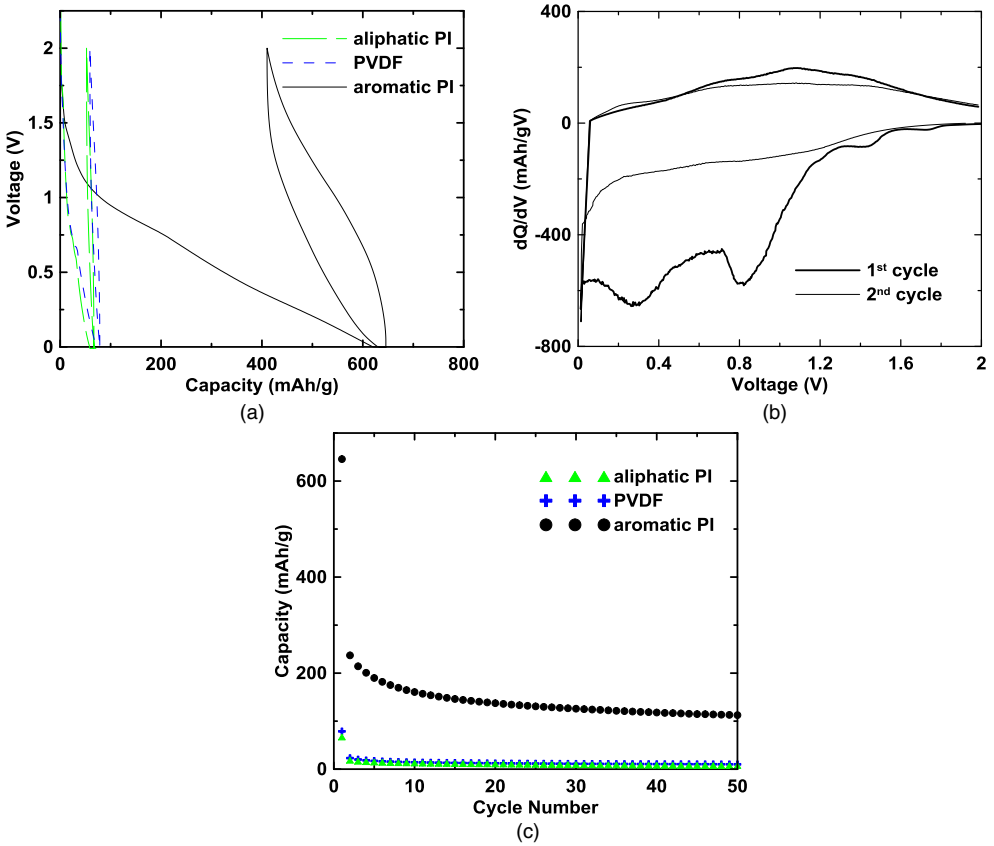

Figure 7. (a) Voltage curves of aro-PI, ali-PI and PVDF binders versus Na-metal as measured in TiN/binder coatings. (b) Differential capacity curve of aro-PI binder versus Na-metal as measured in a TiN/ari-PI coating. The first cycle is shown in bold. (c) Cycling performance of aro-PI, ali-PI and PVDF binders versus Na-metal as measured in TiN/binder coatings.

behavior of aro-PI during lithiation, a major peak in the differential capacity during sodiation occurs, presumably due to SEI formation, which is larger in capacity than for ali-PI or PVDF. In this case, the peak is at about 0.8 V vs. Na (or about 1.1 V vs. Li). This peak is followed by a second peak at 0.3 V vs. Na, which may be from the reduction of aro-PI. After the first lithiation, the differential capacity becomes rather featureless, with indistinct peaks. The cycling performance of the PVDF, ali-PI and aro-PI binders in Na cells is shown in Figure 7c. As in Li cells, aro-PI yields a significantly larger initial discharge capacity and reversible capacity than the other binders. However, these capacities are much smaller than those for aro-PI in Li cells. In Na cells aro-PI has a 645 mAh/g first sodiation capacity, corresponding to a 12 electron reduction and a first desodiation capacity of 235 mAh/g, corresponding to a 4 electron oxidation. These values are much smaller than those found above for TiN/aro-PI versus Li-metal. In addition, TiN/aro-PI versus Na-metal also shows less hysteresis than with lithium.

Although smaller capacities are observed for aro-PI in Na cells than Li cells, the capacities are still very large and suggest the aro-PI undergoes an irreversible decomposition during sodiation. Interestingly, the lower initial capacities and hysteresis of aro-PI in a Na cell compared to its behavior in a Li cell is similar to the behavior of a hydrogen containing carbon, which also shows lower capacity and hysteresis in Na cells compared to Li cells.[21] We therefore speculate that a similar mechanism occurs for aro-PI in Na cells as we have suggested for Li cells in Reaction 2 in which aro-PI decomposes during sodiation to form a hydrogen containing carbon. However, in this case the hydrogen containing carbon will have much reduced capacity and hysteresis with Na than in Li cells.

Since aro-PI has such a high capacity in both Li and Na cells it can contribute significant capacity during cell cycling. The above measurements of binder electrochemistry are important as they can be used to estimate the binder contribution to the total negative electrode capacity, as will be shown below.

Binder performance in graphite coatings.— Figure 8 shows the voltage curves of graphite with aro-PI, ali-PI, and PVDF binders versus lithium metal. Graphite electrodes with PVDF and ali-PI binders have low irreversible capacity. In contrast, the aro-PI cells have a larger first cycle capacity, larger irreversible capacity and additional capacity above 1 V. This extra capacity coincides with the considerable electrochemical activity of aro-PI found in TiN/aro-PI coatings, as discussed in the previous section. The cycling performance of the graphite/binder electrodes are shown in Figure 9 and all have good cycling performance. As expected from the electrochemical activity of aro-PI observed above, the reversible capacity of the electrode with aro-PI binder is significantly higher than the other electrodes, and is about ~382 mAh/g. This is higher than the theoretical value for graphite (372 mAh/g) and also agrees with the findings of a previous study of graphite electrodes with PI binders,[13] which reported that aro-PI contributes to the reversible capacity.

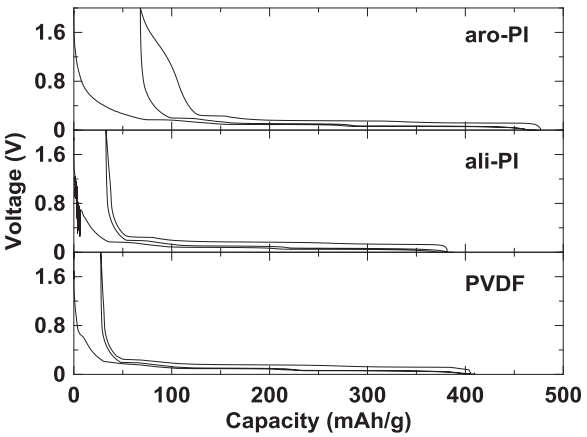

Figure 8. Voltage curves of graphite electrodes with aro-PI, ali-PI and PVDF binders versus Li-metal.

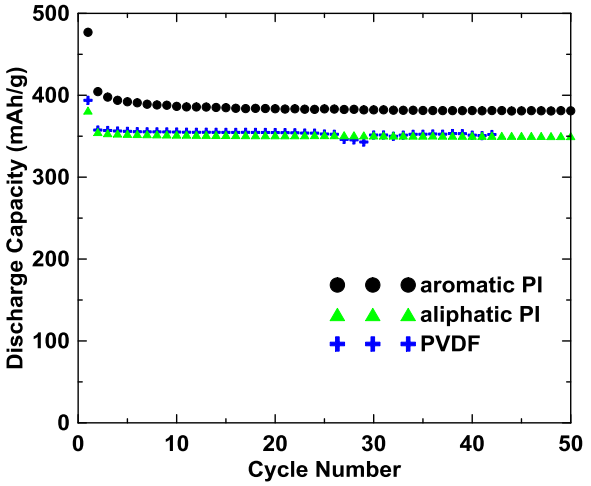

Figure 9. Cycling performance (discharge capacities) of graphite electrodes with aro-PI, ali-PI and PVDF binders versus Li-metal.

In order to see if the observed electrochemical behavior of aro-PI in a TiN/aro-PI coating reflects the behavior of aro-PI in a graphite/aro-PI coating, the cycling performance of the graphite/aro-PI coating is compared to that of a graphite/ali-PI coating in Figure 10. Also shown is capacity vs cycle number plot derived from the capacity of aro-PI as measured in a TiN/aro-PI coating (shown in Figure 3c) added to the graphite/ali-PI coating in an amount corresponding to the weight percent of aro-PI in the graphite/aro-PI coating. Since the ali-PI is not electrochemically active, then adding the capacity of aro-PI found the TiN/aro-PI coating shown in Figure 3c to the capacity of the graphite/ali-PI coating should result in a capacity that is the same as the graphite/aro-PI coating. This was indeed found to be the case. The agreement between the predicted capacity graphite/aro-PI electrode capacity and its actual capacity is very good. This data confirms that the cycling performance measured for aro-PI in TiN/aro-PI coatings is representative of the behavior of aro-PI in active composite coatings.

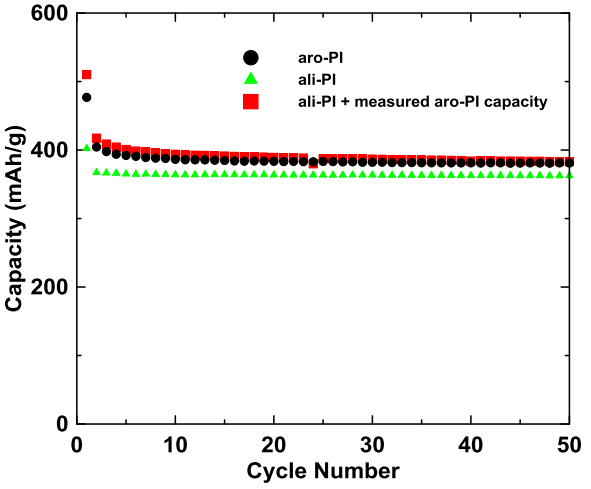

Figure 10. Capacity vs. cycle number plotted for a graphite/aro-PI coating and a graphite/aro-PI coating vs. Li. Also shown is the predicted capacity of the graphite/aro-PI coating calculated by adding the irreversible and reversible aro-PI capacity (as measured from TiN/aro-PI coatings) to the graphite/ali-PI electrode capacity.

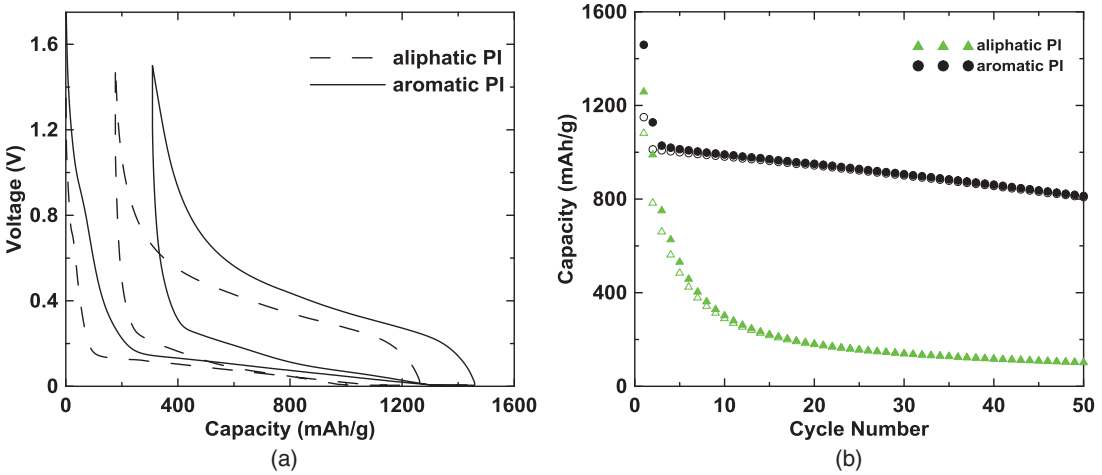

Figure 11. Voltage curves of V6 alloy electrodes with ali-PI and aro-PI binders versus Li-metal. (b) Cycling performance of V6 alloy electrodes with ali-PI and aro-PI binders versus Li-metal.

aro-PI and ali-PI binder performance in alloy coatings for Li-ion cells.— The cycling performance of V6 alloy was evaluated in V6/carbon black/binder electrodes using aro-PI and ali-PI binders in Li cells. Figures 11a and 11b show the first cycle voltage curves and cycling performance of these electrodes, respectively. The alloy electrode with aro-PI binder has good cycling characteristics for this coating formulation, and it is well known now that aro-PI is a good binder in alloy coatings.[3–5] However, the alloy electrode with aro-PI binder has high irreversible capacity, which is expected from the active aro-PI binder contribution. The alloy electrode with ali-PI binder has much lower first cycle capacity and irreversible capacity, which is consistent with the findings above that ali-PI is inactive, however the cycling performance of the alloy electrode with ali-PI binder is very poor. In order to better demonstrate the good cycling performance of alloy electrodes with aro-PI binder, Figures 12a and 12b show the voltage curve and cycling performance of an optimized coating formulation that includes graphite, according to Du et al.[22] This electrode has no capacity fade in the 50 cycles shown.

aro-PI binder performance in Na cells.— Figure 13a shows the voltage profiles of hard carbon in electrodes using aro-PI, ali-PI, and PVDF binders in Na cells. Voltage curves of the same electrodes in Li cells are shown for comparison. As expected from the results of TiN/binder coatings above, the cells with aro-PI have a greater first discharge capacity and greater reversible capacity than those with PVDF. The capacity increase is much greater for Li cells than for Na cells (150 versus 50 mAh/g, respectively on first discharge), also as expected. The cycling performance of these coatings is shown in Figure 13b. All electrodes have good cycling characteristics, excepting the hard carbon electrode with aro-PI binder in a Li cell, which shows some fade. This fade is likely from the aro-PI binder, makes up a significant portion of the capacity and has significant fade, as shown in Figure 3c. All of these results are consistent with the measured electrochemistry of aro-PI and ali-PI in TiN/binder coatings discussed above.

Similar to alloy electrodes in Li-ion cells, we have found that aro-PI works well as a binder for alloy electrodes for Na cells. For instance, Qian et al. investigated a Sb/C nanocomposite in room temperature Na-ion batteries. They found it to have good cycling performance using CMC binder.[16] Figure 14 shows the X-ray diffraction pattern of Sb/C nanocomposite synthesized in this study. The observed peaks correspond to a rhombohedral phase of Sb.[23] No peaks were observed corresponding to any carbon phase, indicating that the carbon is amorphous. This is consistent with a previous study by Qian et al.[16] Figure 15 shows the cycling performance of the Sb/C nanocomposite with aro-PI binder versus Na-metal. To be consistent with Ref. 16, the capacity is calculated with respect to the Sb content of the coating only. A large irreversible capacity is observed; the initial discharge/charge capacities are 872/662 mAh/g. Good cycling performance is obtained in the 50 cycles shown.

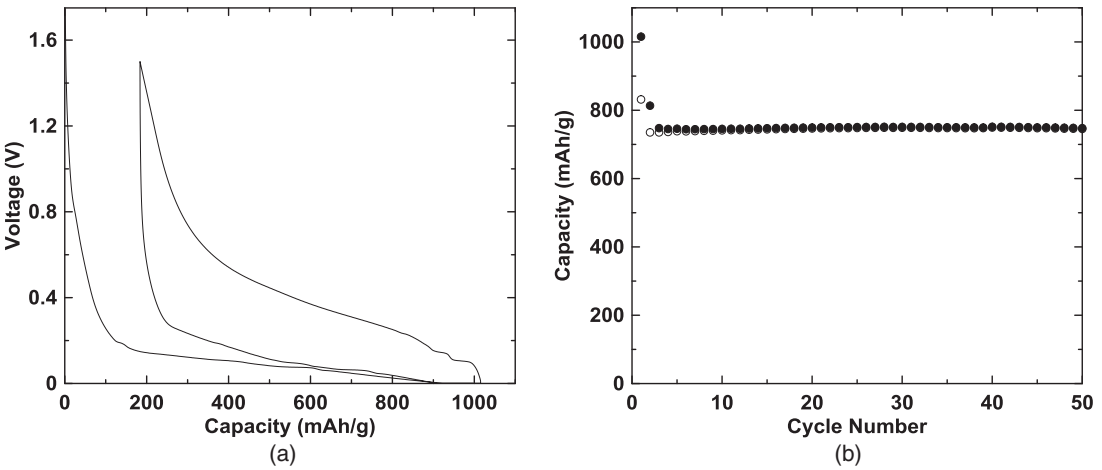

Figure 12. (a) Voltage curve and (b) cycling performance of a V6/graphite electrode with aro-PI binder versus Li-metal.

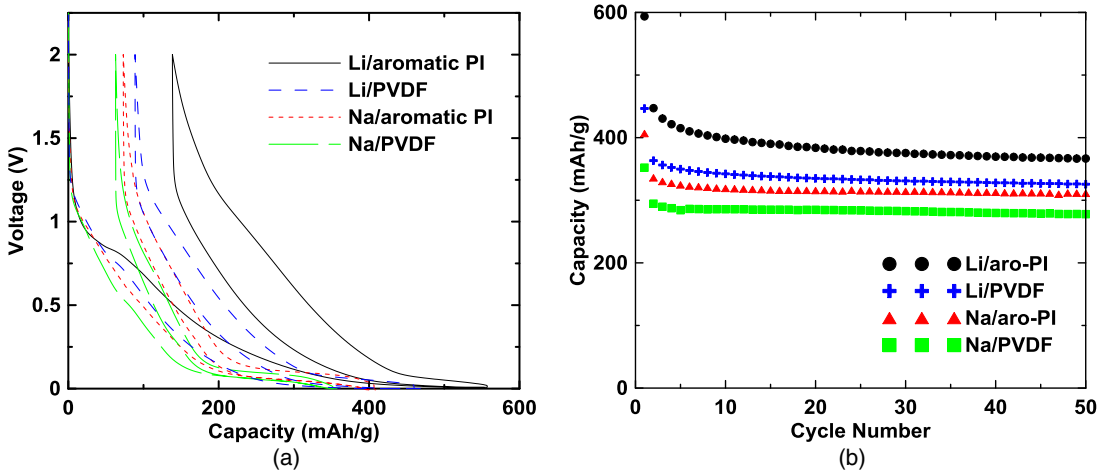

Figure 13. (a) Voltage curves of hard carbon electrodes with aro-PI and PVDF binders versus Li and Na-metal. (b) Cycling performance of hard carbon electrodes with aro-PI and PVDF binders versus Li and Na-metal.

Discussion

The high initial capacity measured for aro-PI in Li and Na cells is strongly suggestive that these polymers undergo an almost complete reductive decomposition at low voltages. The voltage curves of the products after the first lithiation are consistent with the formation of hydrogen containing hard carbons. ali-PI, on the other hand, is practically electrochemically inert. It is likely that the initial 2-electron reduction of aro-PI imposes electrical conductivity on the polymer, making it susceptible to reduction, while ali-PI remains non-conducting and inert. The good binder properties of aro-PI in alloy electrodes, then, must be attributed to its decomposition products, which are not formed by ali-PI. When aro-PI is reduced during its first lithiation, it probably forms a conductive carbon layer around the alloy particles, which apparently is beneficial for cycling. This would suggest that electrodes with carbonized binders might perform well in alloy cells. We have indeed found this to be the case and will show that alloy electrodes with thermally carbonized binders cycle well in a subsequent publication.

These findings have profound implications for the use of binders in alloy coatings. We note that conductive polymer binders previously studied in alloy coatings also show anomalously high first lithiation capacities, high irreversible capacities, and additional high voltage capacity during their first lithiation.[2,24] For instance, an additional first cycle capacity of 500 mAh/g for a Si nano-particle PANi hydrogel composite coating was attributed to SEI formation.[2] However, the large magnitude of this high voltage capacity is difficult to reconcile with SEI formation. Unfortunately, there are no voltage curves in these studies comparing these electrodes with those containing inactive binders, so that the additional first cycle capacity cannot be properly quantified. We suggest that such studies are needed, since from the behavior of aro-PI shown here, we suspect that such conductive polymers may simply be decomposing to carbon during their first cycle. If this is the case, much more inexpensive polymers might be just as effective.

Conclusions

The electrochemistry of aro-PI and ali-PI binders were carefully measured in TiN/binder composite coatings. Such coatings can measure the electrochemistry of binders in the same morphology as they are used in composite coatings with active materials. The lithiation and sodiation behavior of aro-PI was consistent with its almost full decomposition to a hydrogen containing carbon. After this first lithiation or sodiation, a reversible voltage curve that also resembled a hydrogen containing carbon was observed in both lithium and sodium cells. This reduction causes coatings with aro-PI binder to have high

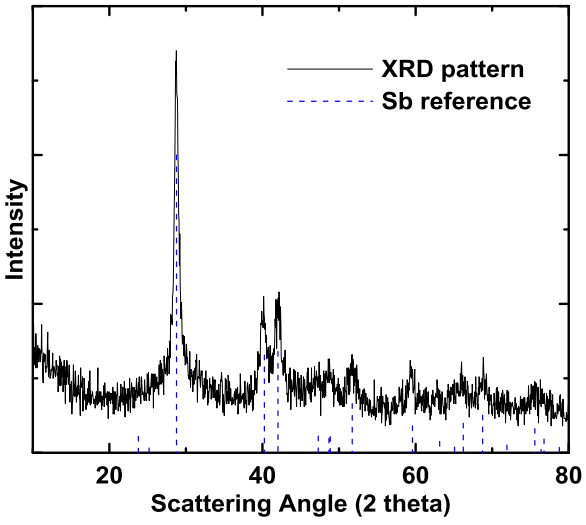

Figure 14. X-ray diffraction pattern of Sb/C nanocomposite synthesized by ball milling antimony and carbon black powders for 11 hours. The known peak positions of antimony are indicated by blue lines.[23]

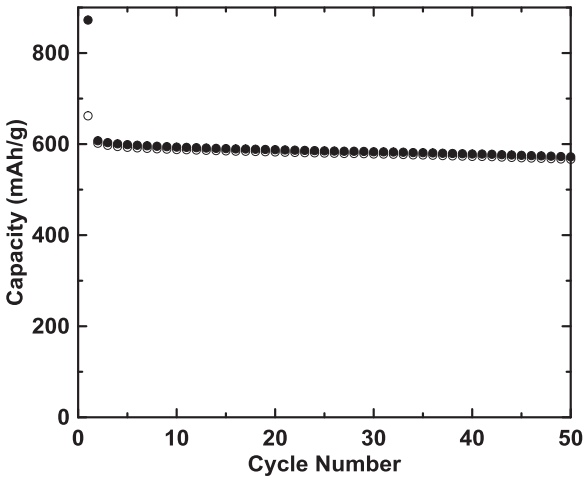

Figure 15. Cycling performance of a Sb/C nanocomposite / aro-PI binder electrode versus Na-metal.

irreversible capacity and also additional reversible capacity during cycling, compared to inactive binders.

In contrast to aro-PI, ali-PI was found to be electrochemically inert and alloy electrodes with ali-PI cycle poorly. We therefore attribute the good cycling properties of alloy electrodes with aro-PI binder to its decomposition products that form during lithiation, which we suspect to be hydrogen-containing carbons. This may also suggest that conductive polymers used as binders in the past may also be decomposing to carbon during their first lithiation. Further studies are needed to confirm the decomposition of such binders, since much less expensive alternatives may be available, if the good performance of conductive polymers in alloy electrodes is only due to their decomposition products.

References

1. M. N. Obrovac and V. L. Chevrier, *Chemical Reviews*, **114**, 11444 (2014).
2. H. Wu, G. Yu, L. Pan, N. Liu, M. T. McDowell, Z. Bao, and Y. Cui, *Nature Communications*, **4**, 1943 (2013).
3. A. Guerfi, P. Charest, M. Dontigny, J. Trottier, M. Lagacé, P. Hovington, A. Vijh, and K. Zaghib, *Journal of Power Sources*, **196**(13), 5667 (2011).
4. J. S. Kim, W. Choi, K. Y. Cho, D. Byun, J. Lim, and J. K. Lee, *Journal of Power Sources*, **244**, 521 (2013).
5. Q. Yuan, F. Zhao, Y. Zhao, Z. Liang, and D. Yan, *Journal of Solid State Electrochemistry*, **18**(8), 2167 (2014).
6. C. Sroog, *Journal of Polymer Science: Macromolecular Reviews*, **11**(1), 161 (1976).
7. J. Li, *Advanced Negative Electrodes for Lithium-Ion Batteries*, Dalhousie University, 2009.
8. A. Viehbeck, M. Goldberg, and C. Kovac, *Journal of The Electrochemical Society*, **137**(5), 1460 (1990).
9. G. Rabilloud, in, *High Perform. Polym.*, 3rd ed., Editions Technip, (2000), p. 121.
10. N. S. Hochgatterer, M. R. Schweiger, S. Koller, P. R. Raimann, T. Wöhrle, C. Wurm, and M. Winter, *Electrochemical and Solid-State Letters*, **11**(5), A76 (2008).
11. J.-S. Bridel, T. Azaï, S. M. Morcrette, J.-M. Tarascon, and D. Larcher, *Journal of The Electrochemical Society*, **158**(6), A750 (2011).
12. S. Mazur, P. Lugg, and C. Yarnitzky, *Journal of The Electrochemical Society*, **134**(2), 346 (1987).
13. N. Ohta, T. Sogabe, and K. Kuroda, *Carbon*, **39**(9), 1434 (2001).
14. N.-S. Choi, K. H. Yew, W.-U. Choi, and S.-S. Kim, *Journal of Power Sources*, **177** (2), 590 (2008).
15. L. J. Krause, L. D. Jensen, and Polyimide Electrode Binders, U.S. Pat. US 7, 972, 725 B2, 2011.
16. J. Qian, Y. Chen, L. Wu, Y. Cao, X. Ai, and H. Yang, *Chemical Communications*, **48**(56), 7070 (2012).
17. C. A. Schneider, W. S. Rasband, and K. W. Eliceiri, *Nature Methods*, **9**, 671 (2012).
18. I. Kim, P. N. Kumta, and G. E. Blomgren, *Electrochemical and Solid-State Letters*, **3**(11), 493 (2000).
19. G. Cui, L. Gu, A. Thomas, L. Fu, P. a van Aken, M. Antonietti, and J. Maier, *ChemPhysChem*, **11**(15), 3219 (2010).
20. T. Zheng, W. R. McKinnon, and J. R. Dahn, *Journal of The Electrochemical Society*, **143**(7), 2137 (1996).
21. D. A. Stevens and J. R. Dahn, *Journal of The Electrochemical Society*, **148**(8), A803 (2001).
22. Z. Du, R. A. Dunlap, and M. N. Obrovac, *Journal of The Electrochemical Society*, **161**(10), A1698 (2014).
23. ICSD Reference: 00-085-1322 ICSD Using POWD-12++, **16**, 451 (1997).
24. S. Xun, X. Song, V. Battaglia, and G. Liu, *Journal of The Electrochemical Society*, **160**(6), A849 (2013).